

# The annular glow discharge: a small-scale plasma for solution analysis

Michael R. Webb, Francisco J. Andrade and Gary M. Hieftje\*

Received 13th November 2006, Accepted 9th May 2007

First published as an Advance Article on the web 29th May 2007

DOI: 10.1039/b616521d

A recent trend in plasma spectrochemistry, and in analytical chemistry in general, has been towards miniaturization. Miniaturized plasma sources often have properties leading to low cost, potential portability, and simplified integration with separation instrumentation such as chromatographs. However, these discharges have not often performed well with solution samples. To address this shortcoming, we have developed a new, small-scale ( $5 \times 2$  mm) plasma, maintained in atmospheric-pressure helium between a tubular cathode and a rod-shaped anode (both made of steel). The discharge extends between the two electrodes and an annular glow is visible within the cathode tube. An aerosol is introduced into the plasma through the cathode, and atomic emission is observed in the near-cathode region. In this study, we observe the effects of solvent addition on the plasma in terms of its electrical and spectroscopic characteristics and how they change with solution flow rate. Given that even a robust source such as the inductively coupled plasma is different under wet and dry conditions, it is not surprising that the discharge introduced here is affected by the presence of an aerosol. However, the discharge is stable even with significant solvent loading. In this preliminary investigation, flow injection has been used to establish detection limits for several metals between 7 ppb (0.7 ng absolute) for Cd and 111 ppb (11 ng absolute) for Cu.

## Introduction

Inductively coupled plasmas (ICPs) are well known for their usefulness in analyzing solution samples, but they are the exception rather than the rule for plasmas. Microwave plasmas and low pressure glow discharges, for example, lack the thermal energy or aerosol residence time necessary for efficient desolvation.<sup>1,2</sup> Even when plasmas have regions with high thermal energy, properties of the plasma can prevent aerosols from effectively penetrating into these regions. An apt example is the ICP itself. At lower frequencies (*e.g.* 5 MHz), a spheroidal plasma forms, and gas expansion near this region pushes much of the aerosol towards the cooler outer region of the plasma.<sup>1,2</sup> At the frequencies now typically used (27 and 40 MHz) and with a high gas velocity through the centre of the ICP, an annular plasma forms more easily, and much of the aerosol is channelled to the centre, which is cooler than the annular region but still quite hot.<sup>1-3</sup>

A recent trend in analytical chemistry has been towards miniaturization, and researchers involved with plasma spectrochemistry have followed this trend with an array of miniaturized plasmas, mostly designed for atomic or molecular detection of gas chromatography effluents.<sup>4-6</sup> Motivations for the development of such plasmas are mostly related to cost, potential for portability, and integration with chromatographic and other separation instrumentation. Typical properties of these plasmas that address those motivations are small footprint, low gas and power consumption, low construction

costs, and the lack of a need for vacuum equipment. Attention is sometimes focused on plasmas with at least one dimension below an arbitrary 1 mm cut-off (which are commonly classified as microplasmas even when they have other dimensions of several millimetres or even a few centimetres), but the advantageous traits of miniaturized plasmas should not be expected to obey this sharp distinction.

Reviewers of the field seem encouraged by recent progress with gaseous samples, but tend to be considerably less optimistic when solution sample introduction is used,<sup>4-6</sup> at least in the absence of nearly complete separation of the analyte from the liquid solvent. This requirement is typically ill-suited for continuous analysis and ordinarily involves the use of transient sample introduction (*e.g.* electrothermal vaporization)<sup>6</sup> or requires different conditions for different analytes (*e.g.* hydride generation).<sup>7</sup> Perhaps because of a combination of shorter residence times and lower gas temperatures, miniaturized plasmas tend to have even more difficulty with solution samples than their larger cousins. In fact, they often become unstable or are extinguished when an aerosol is added. By the standards of solution analysis with miniaturized plasmas, a significant accomplishment is the miniaturized ICP (described by its inventors as an atmospheric-pressure microplasma jet).<sup>6,8</sup> This device achieves a detection limit of 5 ppm for sodium with electrospray sample introduction but does not tolerate the higher solvent loads of even a micronebulizer.

It should be noted that successful solution analysis by miniaturized plasmas has been accomplished by means of variations on glow discharge electrolysis (GDE), an electrochemical technique discovered by Gubkin in 1887.<sup>9</sup> In GDE, a glow discharge is maintained with at least one electrode consisting of an electrolytic solution. Notable applications of

Department of Chemistry, Indiana University, Bloomington, IN 47405, USA. E-mail: hieftje@indiana.edu; Fax: +1-812-855-0958; Tel: +1-812-855-2189

this technique to atomic emission spectrometry include the electrolyte-cathode discharge (ELCAD)<sup>10–12</sup> and the liquid-sampling atmospheric-pressure glow discharge (LS-APGD).<sup>13,14</sup> In both of these techniques, the cathode is typically the solution sample. In all GDE-based techniques, the emission is highly dependent on the electrolyte concentration, which leads to two constraints that can be disadvantages: solutions must have high electrolyte concentrations for good sensitivity and these concentrations must be highly consistent between standards and samples if acceptable quantification is desired.<sup>11,13</sup>

In the present work, we introduce a miniaturized plasma that is stable even with a significant solvent load. This plasma belongs to a general class of atmospheric-pressure helium discharges.<sup>15</sup> One such discharge reported in the literature is capable of elemental analysis of aerosols, but this discharge uses an order of magnitude higher power and achieves detection limits significantly worse than the source presented here.<sup>16</sup> In our experience, tolerance to solvent loading is not a general property of these discharges. It is likely that the particular geometry of the source presented here is the factor that allows it to perform so well, just as the ICP geometry contributes to its success. In this new source, a sample aerosol is directed through a tubular cathode, within which there is an annular negative glow. For this reason, we describe this as an annular glow discharge (AGD). This source differs from a classical hollow cathode glow discharge, in which the negative glow is spheroidal.

## Experimental

The experimental setup for the new source is shown in Fig. 1. Sample solutions were supplied by a PHD-2000 syringe pump (Harvard Apparatus, Holliston, MA, USA) and the flow of ultra-high-purity helium (Airgas, Inc., Radnor, PA, USA) was regulated by a Tylan model FC-280 mass flow controller. Helium flow was maintained at 1.5 L min<sup>-1</sup>. Sample solutions were prepared from DI water. Both were fed through a Meinhard (Golden, CO, USA) TR-50-A1 concentric nebulizer. Large droplets were removed from the resulting aerosol by a Wu-Hieftje vertical rotary spray chamber (LECO, St. Joseph, MI, USA), which was drained by a Perkin-Elmer (Norwalk, CT, USA) Minipuls 2 peristaltic pump. After the spray chamber, the aerosol passes through a 45 mm long, 5 mm diameter glass tube. The glass tube is connected through a male-male Swagelok<sup>®</sup> connector to a brass chamber, which is wrapped in glass wool for thermal insulation. The chamber

is 11 mm in diameter and 8 cm long. The cathode, a 2 mm inner-diameter steel tube, screws into the other end of the brass chamber. The anode is a 7.4 mm diameter steel rod with a rounded tip. The anode and cathode are separated by 5 mm at a slight angle so the discharge contacts the anode approximately 0.5 mm off the axis of the cathode. This arrangement was adopted to simplify axial viewing.

The discharge was powered by a Kepco (Flushing, NY, USA) 1000 BHK-0.2MG high voltage power supply. A positive potential was supplied to the anode and the cathode was grounded. Two 1.25 k $\Omega$  resistors were placed in series with the anode and the power supply to stabilize the discharge. Typical power usage was 75 W, with 40 W dropped across the plasma. For DC voltage measurements, a Fluke (Everett, WA, USA) model 175 digital multimeter was used in combination with a Fluke 80K-40 high-voltage probe. For the measurement of noise power spectra, a Tektronix (Richardson, TX, USA) TDS 2024 digital oscilloscope was used in combination with an AK-510 high-voltage probe (R. S. R. Electronics, Inc., Avenel, NJ, USA); a fast Fourier transform was performed by the oscilloscope using its flat-top algorithm. For current measurements, a 2.1  $\Omega$  resistor was placed in series with the discharge, between the cathode and ground, and the potential drop across it was converted to current through it by means of Ohm's law. This voltage measurement was made using a Tektronix DM252 multimeter.

An Ocean Optics (Dunedin, FL, USA) USB2000 spectrometer with a fibre optic attachment was used to determine what region of the plasma produced analyte emission; the arrangement used in this study was based on the observation that emission is strongest in the near-cathode region. The emission was measured nearly on-axis to the cathode, but at an approximately 9° angle so the anode did not block the light from reaching the spectrometer. A 7 cm focal length fused-silica lens focused light onto the monochromator entrance slit with a magnification of approximately 0.36. The monochromator was a McPherson (Chelmsford, MA, USA) EU-70 unit with 50  $\mu$ m slits, providing 0.1 nm resolution. The current from a Hamamatsu (Hamamatsu, Japan) R928 photomultiplier tube was converted to voltage by a Keithley (Cleveland, OH, USA) 427 Current Amplifier. The voltage was recorded with LabVIEW (National Instruments, Austin, TX, USA). Fast Fourier transforms were performed by a LabVIEW program that normalized the emission before the power spectra were calculated, using a flat-top algorithm.

## Results and discussion

### Visual observations

In the following description, the cathode axis is defined as the central axis of the cathode tube (*i.e.*, the axis parallel to the cathode's inner and outer walls). A bright annular glow, believed to be the negative glow, is observable inside the cathode. Its outer diameter is such that no space is visible between it and the inner wall of the cathode (2 mm diameter), although there is presumably a dark space on the scale of single to tens of micrometres in thickness.<sup>17</sup> The glow itself appears to be a few hundred micrometres thick, leaving a dark

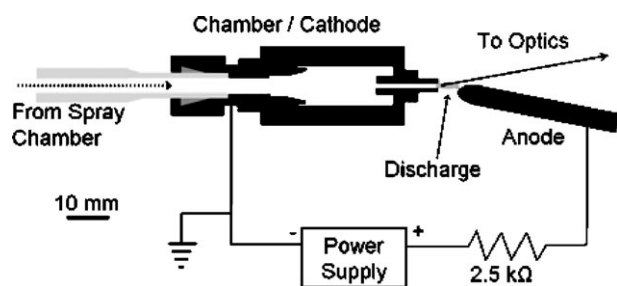


**Fig. 1** Diagram of annular glow discharge. Upper portion is approximately to scale. Black areas are metals (brass or steel).

central channel between 1 and 1.5 mm in diameter. A glow, possibly the positive column, also extends between the cathode and the anode. Near the cathode, this second glow is mostly diffuse and dim, except for one thin brighter region starting near the cathode wall and extending at a slight angle to the cathode axis so that it intersects this axis about 3 mm from the cathode. Between the cathode and this intersection point, the bright region becomes more diffuse and, by the intersection point, the dim diffuse and bright thin regions have merged into a single bright diffuse region. This region extends along the cathode axis until the anode, at which point it bends sharply to intersect the anode, which lies half a millimetre off the cathode axis in the arrangement studied here. This diffuse region is about 2 mm in diameter at the anode. On the anode surface, there is another bright glow. This region is very thin and perpendicular to the anode surface, but takes the form of an ellipse in the plane parallel to the anode surface. Note that the anode surface contacted by the discharge is not perpendicular to the cathode axis but is nearly parallel to it and also that this surface is curved rather than flat. The ellipse is elongated (about 3 mm) in the direction nearly parallel to the cathode axis compared to the direction nearly perpendicular to it (about 2 mm). Between the diffuse region and the anode glow, there appears to be a dark region, but its small size (perhaps less than 100  $\mu\text{m}$ ) makes it difficult to observe. A photo of the discharge can be found with the contents entry for the present manuscript.

Although the thin bright region often remains stably anchored to one spot on the cathode for periods of several hours of continuous operation, it can also become unstable, hopping between two points with periods of hundreds of milliseconds to minutes. This instability is obviously detrimental to analytical measurements because movement of the bright zone into and out of the region imaged onto a spectrometer entrance aperture will change the emission intensity measured by that spectrometer. It is not clear at present why the region anchors to a particular spot or what causes it to hop, but it is clearly something that would be desirable to control. Work to overcome this instability is currently under way. All of the measurements presented here were performed while the bright region was stably anchored to a single spot.

When an aerosol is introduced through the tubular cathode, the thin bright region becomes more diffuse and less distinct from the dimmer diffuse region. Aside from this change, the description of the dry discharge holds.

These discharge regions certainly merit further study, but this coverage would be outside the scope of the present work. However, they appear to be highly analogous to the regions of another atmospheric pressure helium discharge, which was studied by Andrade *et al.*<sup>15</sup> It also should be noted that, based on observations with the Ocean Optics spectrometer and on imaging the source onto the slit of a monochromator from different angles, the majority of analyte (metals introduced in the aerosol) emission is from near or within the cathode tube.

### Electrical characterization

The electrical characteristics of the plasma under a range of solvent loads can be seen in Fig. 2. Let us first consider the dry

plasma. The slope of this plot, the dynamic resistance, is negative. It should be noted that there is a voltage drop across the ballast resistors that is not included in this measurement and is large enough to make the total resistance positive; this feature serves to stabilize the plasma. Negative resistance is ordinarily seen as an indication of an arc rather than a glow discharge, but the magnitudes of the current and voltage here are atypical for an arc. Also, under certain conditions, similar plasmas have shown a positive resistance or a resistance that changes from negative to positive with increasing current.<sup>15</sup> It seems likely then, that there are two or more processes occurring with opposing resistances. Positive dynamic resistance is a familiar property of an abnormal glow discharge and is described elsewhere,<sup>17–19</sup> so it merits little description here. In an abnormal glow discharge (a discharge in which the available cathode surface is covered by the discharge as is typical in analytical spectroscopy), increases in the current density require greater potentials, imparting a positive dynamic resistance.<sup>17–19</sup> In a normal glow discharge, where the available cathode is not completely covered, zero dynamic resistance is found because higher currents increase the cathode-surface coverage rather than the current density. The negative resistance here might be explained in part by Joule heating,<sup>17</sup> which grows as current density rises; in turn, the consequently higher temperature lowers the density of the gas and therefore reduces the potential required to maintain a glow discharge.<sup>17,18</sup> Whether or not this heating plays a role in the observed behaviour, this negative dynamic resistance is common among atmospheric pressure glow discharges with large positive columns.<sup>15,20</sup>

When the influence of solution flow rate on the discharge (for example, Fig. 2) is interpreted, it is important to realize that the solvent transport efficiency climbs rapidly as flow rate decreases, such that it is only a few percent at a typical flow rate of 1 mL min<sup>-1</sup> but can be as high as 80% at very low flow rates (10  $\mu\text{L min}^{-1}$ ).<sup>21</sup> Of course, these values will vary with the nebuliser–spray chamber combination, the gas flow, and the nebuliser-gas identity.<sup>22–24</sup> The result is

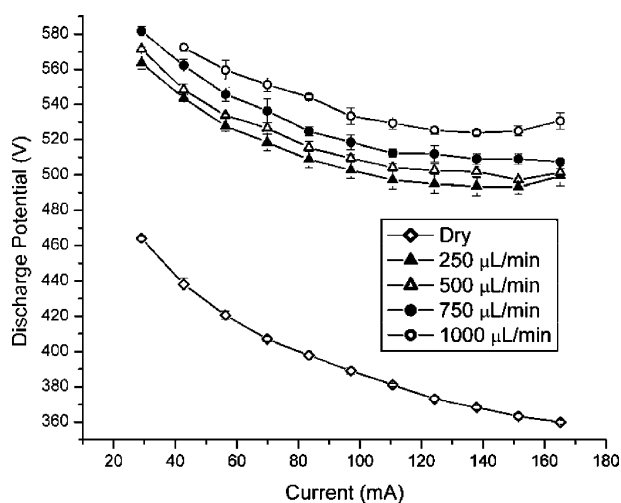
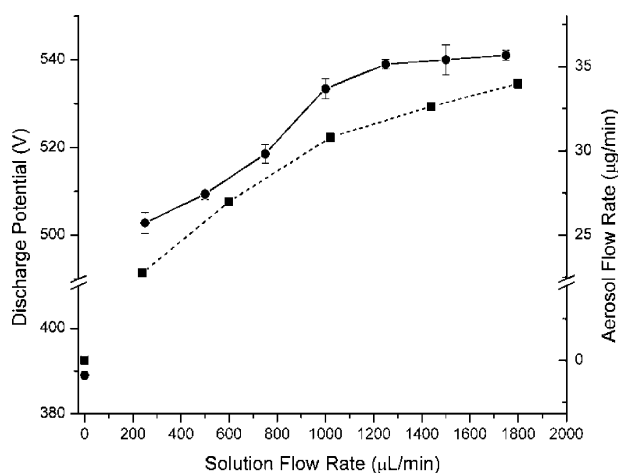


Fig. 2 Electrical characteristics of the annular glow discharge under different solution (DI water) flow rates. Error bars represent twice the standard deviation of 5 measurements.

that the mass of solvent leaving the spray chamber and entering the discharge (the aerosol) does not scale linearly with solution flow rate and varies relatively little across the flow range used here.

To test the relationship between solution and aerosol flow rates, a U-shaped tube filled with Drierite (Xenia, OH, USA) 8 mesh anhydrous calcium sulfate was attached to the output of the spray chamber to trap the aerosol. The mass change was measured and divided by the time to establish the aerosol flow rate. The results are plotted as aerosol flow rate *vs.* solution flow rate in Fig. 3 (squares connected by dashed lines; right axis). Between solution flow rates of 240 and 1800  $\mu\text{L min}^{-1}$  (a 650% increase), the aerosol flow rate only changes from 22.8 to 34.0  $\mu\text{g min}^{-1}$  (a 49% increase).

There are two notable effects of the aerosol on the electrical characteristics of the annular discharge. The first is that the potential, and therefore the power, required to maintain a given current is greater as the sample-solution flow rate is raised. This behaviour is best shown in Fig. 3. The second, shown in Fig. 2, is that the dynamic resistance becomes somewhat less negative, then slightly positive, at high currents under higher solution flow rate conditions. Molecular gases, such as water, provide a larger number of pathways for energy loss (*e.g.* electronic, vibrational, and rotational excitation) than do atomic gases, therefore in the presence of molecular gases, electrons are more likely to lose their energy before causing ionization, making the breakdown potential higher.<sup>17,25</sup> This higher breakdown voltage elevates the positive resistance. The presence of droplets in the aerosol presumably provides another pathway for energy loss (evaporation), adding to the effect. Changes in the plasma temperature might play some role as well, although the direction of the temperature change and the magnitude of temperature's influence have not yet been established. Possibilities include evaporative cooling, higher power deposition *via* rotational and vibra-



**Fig. 3** Effect of solution (DI water) flow rate on discharge potential (circles with solid lines) and aerosol flow rate (squares with dashed lines). Error bars on discharge potential measurements represent twice the standard deviation of 5 measurements. A current of 100 mA was maintained for potential measurements and the discharge was disconnected for aerosol measurements. Note that the y-axes are not continuous.

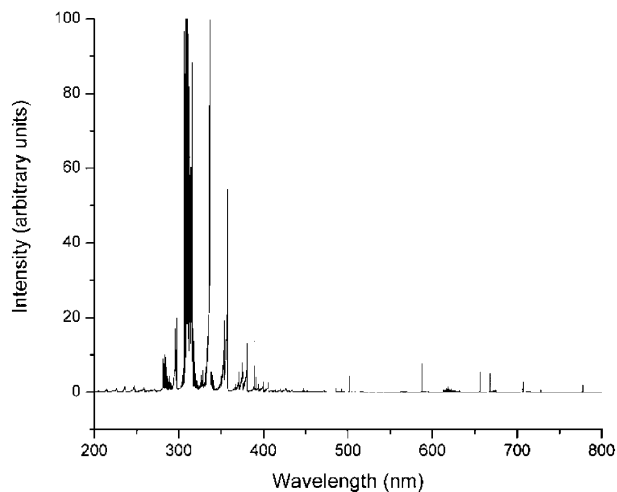


**Fig. 4** Annular glow discharge spectrum with no aerosol or vapour added. Note that emission goes off scale at 309 and 337 nm. A current of 100 mA was maintained.

tional paths which, in turn, lead to heating and cooling by spreading thermal energy through the more diffuse plasma that exists when water is present.

### Spectral features

Fig. 4 and 5 show emission spectra of the annular discharge under dry and wet conditions, respectively. The vertical scales in the two figures are equal and the emission goes off-scale (over 100 arbitrary units) at 309 and 337 nm in Fig. 4. Observable molecular species are NO ( $\gamma$  system with double-headed, blue-degraded bands below 300 nm), OH (red-degraded bands with bandheads at 281 and 306 nm), and  $\text{N}_2$  (blue-degraded bands prominent from 300 to 450 nm). Observable atomic species are the helium atom (388.9, 438.8, 447.2, 471.3, 492.2, 501.6, 504.8, 587.6, 667.8, 706.5, and 728.1 nm), singly charged helium ion (468.6 nm), oxygen (777.2, 777.4, and 777.5 nm), hydrogen (486.1 and 656.3 nm), and

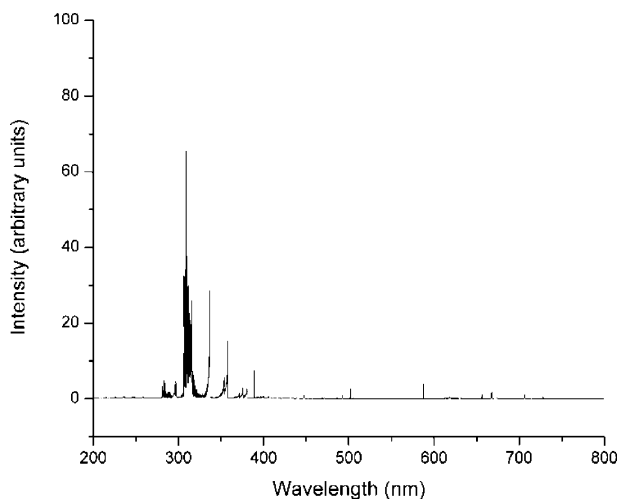


**Fig. 5** Annular glow discharge spectrum with aerosol and vapour resulting from a 500  $\mu\text{L min}^{-1}$  flow of DI water. A current of 100 mA was maintained.

iron (248.3, 248.8, 249.1, 250.1, 251.1, 252.3, 252.7 nm). Most of these features (NO, OH, N<sub>2</sub>, O, and H) can be ascribed to atmospheric gases that are not excluded from the plasma. The helium is obviously the plasma support gas. The iron emission, although weak, is evidence of some erosion of the cathode or anode surface, but emission from other elements in the steel is not seen. It should be noted that although an oxide layer forms on both electrodes, erosion of the surfaces has not been great enough to affect the plasma noticeably.

The measured intensity of all observed background emission features (continuum, molecular, and atomic) declines when aerosol is added. Some of the energy is drained from the plasma in ways that do not lead to emission, such as the evaporation of droplets, but some of this effect is likely due to the discharge becoming more diffuse, leading to a smaller fraction of the total emission being collected through the monochromator entrance slit.

The analyte emission, however, goes up with solution flow rate, as is shown for cadmium in Fig. 6. The trend of this increase is typical for nebuliser-based sample introduction and is the result of a combination of higher analyte input and declining nebuliser efficiency.<sup>21,23</sup> The efficiency of aerosol production drops sharply as flow rate increases, so the amount of analyte reaching the plasma climbs only gradually as solution flow is raised. Although it is likely that there is some depression of the analyte emission at higher solvent loads, this effect is masked by the influence of nebuliser efficiency.

### Noise power spectra

Noise power spectra were collected, under both wet and dry conditions, for the electrical potential (discharge voltage) and for emission of background species. The averages of 15 measurements were plotted for electrical measurements in Fig. 7 and the averages of 24 measurements were plotted for the 309.2 nm OH emission, 587.6 nm He emission, and 228.8 nm Cd emission in Fig. 8, 9, and 10, respectively. A 107.5 Hz peak

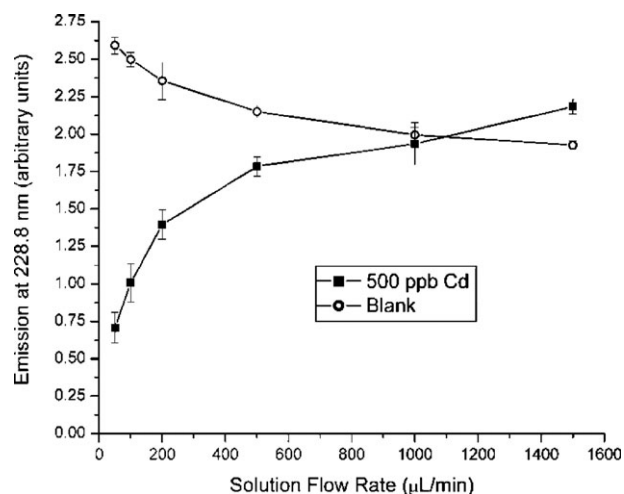


**Fig. 6** Emission of cadmium signal (background-subtracted) and background as a function of solution flow rate. Each point is the average of five 30 s integrations and error bars represent twice the standard deviation of those readings. A current of 100 mA was maintained.

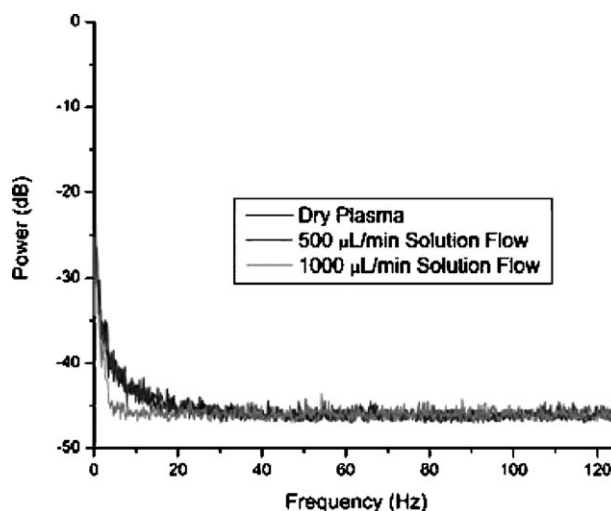


**Fig. 7** Noise power spectra of voltage fluctuations under different solvent (DI water) loads. A current of 100 mA was maintained. Voltage varied with flow rate as in Fig. 3.

in some spectra appears to be environmental noise unrelated to the discharge (it is present even when the discharge is turned off) and its intensity fluctuates. Otherwise, there are no discrete frequencies in the spectra. Rather, the spectra are composed of white and flicker ( $1/f$ ) noise. Although not shown in the figures, frequencies up to 500 Hz have been measured, with no additional features observed aside from harmonics of 107.5 Hz.

Noise spectra measured from some other plasmas often contain sharp features at discrete frequencies.<sup>26,27</sup> However, these features usually arise from the peristaltic pump used for sample introduction or from vortex instabilities surrounding the plasma; a syringe pump was employed here, so the discrete peaks would not be expected.<sup>26</sup> Further, flicker noise in the ICP arises mainly from the sample introduction system.<sup>26,28,29</sup> Given that fact, it is not surprising that the flicker noise in the voltage observed here becomes larger when an aerosol is introduced into the discharge. More surprisingly, the flicker

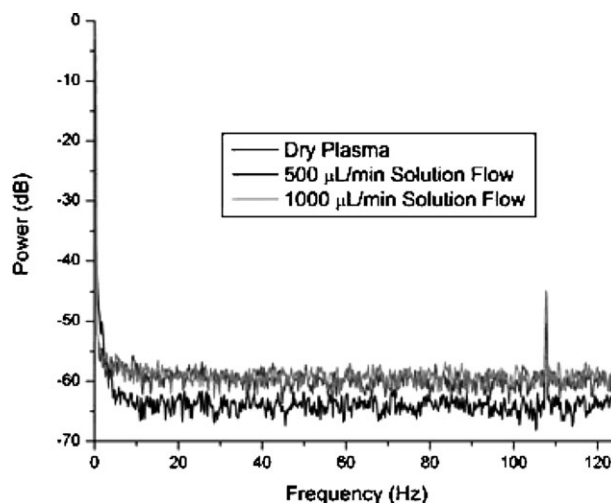


**Fig. 8** Noise power spectra of 309.2 nm OH emission fluctuations under different solvent loads. A current of 100 mA was maintained.

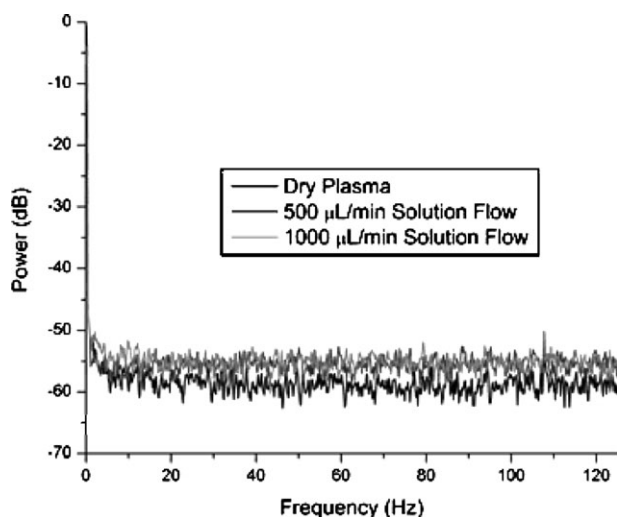


**Fig. 9** Noise power spectra of 587.6 nm He emission fluctuations under different solvent loads. A current of 100 mA was maintained.

noise in emission is not greatly elevated by the addition of aerosol. The white noise, however, does go up slightly in the background emission (OH and He) when solution is added. This increase is no doubt a result of the higher solvent load, which raises OH emission intensity, and the presence of droplets, which produce random fluctuations in most emission features. Probably because the mass of solution making it to the plasma is changed only slightly with the doubling of solution flow rate, there is no observed difference between the noise power spectra for any parameter measured for flows of 500 and 1000  $\mu\text{L min}^{-1}$ .

### Analytical performance

Our preliminary work has concentrated on broad characterization of the plasma and on the influence of an aerosol, but the ultimate goal is to use this discharge for elemental analysis. Consequently, a preliminary evaluation of analytical perfor-

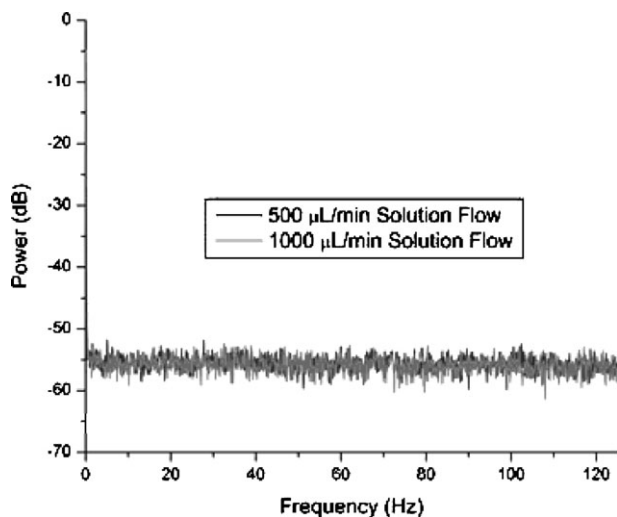


**Fig. 10** Noise power spectra of 228.8 nm Cd emission fluctuations under different solvent loads. A current of 100 mA was maintained.

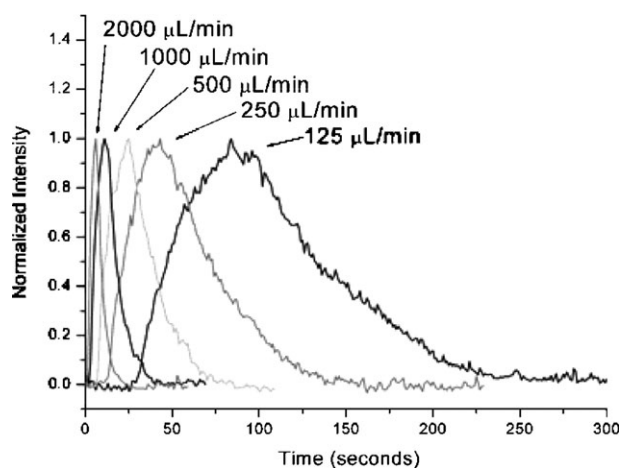


**Fig. 11** Cadmium 228.8 nm signal from 100  $\mu\text{L}$  injections of 500 ppb Cd at different carrier-solution flow rates. A current of 100 mA was maintained.

mance has been made even though the system has not been fully optimized. Because it is intended that this system will be coupled eventually to a separation technique, flow injection was used to test the feasibility of transient analysis. It should be recognized that dilution of the sample, limited integration time, and uncertainty in the synchronization with a manual injection are expected to worsen the analytical performance somewhat compared with continuous injection.

Fig. 11 shows transients for several 100  $\mu\text{L}$  injections of a 500 ppb cadmium solution at carrier flow rates from 125 to 2000  $\mu\text{L min}^{-1}$ . Higher flows were not used because the upper end of this range already exceeds the specifications of the nebuliser manufacturer. The full widths at half maximum are approximately twice what the total duration of the transient would be if there were no broadening, and tailing can be seen. It would certainly be desirable to lessen this broadening, but it would not be prohibitive for many separations. Some broadening can be attributed to spreading between the injection loop and the nebuliser tip, some to the washout time of the spray chamber, and some to the region between the spray chamber and the plasma (because of both the dead volume and the shape). If the last region plays a significant role, reducing its volume in future generations of this discharge should result in narrower transients.

With the carrier solution supplied at 500  $\mu\text{L min}^{-1}$ , 10 injections of 100  $\mu\text{L}$  and 10 injections of a blank were performed for 400 ppb solutions of several metals. A 25 s window encompassing the peak of transient was integrated, and analytical figures of merit, shown in Table 1, were calculated. Detection limits are calculated as the concentration required for a signal three times the standard deviation of the background. Additionally, using triplicate 100  $\mu\text{L}$  injections of 0, 32, 160, 800, and 4000 ppb cadmium, a standard curve with an  $R^2$  of 0.9998 was obtained, showing good linearity for this element over at least 3 orders of magnitude.

It is interesting to compare these detection limits to those of other techniques, particularly the ICP. We can quite readily compare the performance of the instrument used here to complete instruments, but this is not what we are truly

**Table 1** Analytical performance based on 100  $\mu\text{L}$  injections of 400 ppb at a carrier-solution flow rate of 500  $\mu\text{L min}^{-1}$

Element	Wavelength/nm	Detection limit (ppb)	Detection limit/ng	RSD (%)
Cd	228.8	7	0.7	2
Mn	279.5	60	6	10
Mg	285.2	12	1	7
Cu	324.7	111	11	4

interested in. Rather, we would like to compare the two sources (the ICP and AGD), which requires correcting for other differences. Specifically, the resolution of the spectrometer can greatly affect performance.

Boumans and Vrakking<sup>30,31</sup> have examined the dependence of detection limit on spectral resolution. For convenience, an abbreviated treatment is provided here. (Mermet *et al.* have undertaken a similar study, with similar conclusions.)<sup>32</sup>

Two equivalent forms of the detection limit equation are shown below with an intervening step to better demonstrate their equivalence:

$$c_L = kc_0 \frac{\sigma_B}{x_0} = kc_0 \frac{\sigma_B/x_B}{x_0/x_B} = kc_0 \frac{\text{RSD}_B}{\text{SBR}}$$

where  $c_L$  is the concentration detection limit,  $k$  is a constant (we have chosen 3),  $c_0$  is the concentration in the sample,  $\sigma_B$  is the standard deviation of the blank emission,  $x_0$  is the signal (the emission from the sample less the emission from the blank),  $x_B$  is the blank emission,  $\text{RSD}_B$  is the relative standard deviation of the blank, and  $\text{SBR}$  is the ratio of signal to background emission.

When flicker noise dominates,  $\text{RSD}_B$  is independent of spectrometer slit width. Under these conditions, the relationship between spectral bandpass and  $c_L$  is governed by the relationship between spectral bandpass and  $\text{SBR}$ . Boumans and Vrakking arrived at relationships between the  $\text{SBR}$  and the effective line width ( $\Delta\lambda_{\text{eff}}$ ). Which relationship holds depends on the relative magnitudes of the physical line width ( $\Delta\lambda_{\text{phys}}$ ) and the instrumental bandpass ( $\Delta\lambda_{\text{instr}}$ ), which combine to form the effective bandpass:

$$\Delta\lambda_{\text{eff}}^2 = \Delta\lambda_{\text{phys}}^2 + \Delta\lambda_{\text{instr}}^2$$

In situations where the physical line width is greater than twice the instrumental bandpass, the signal increases proportionally to bandwidth, and the background increases proportionally to the square of the bandwidth, making the  $\text{SBR}$  inversely proportional to the effective line width.<sup>30,31</sup> The value of this relationship is that it enables us to predict the  $\text{SBR}$ , and therefore the detection limit that would be expected with the same source but a different spectrometer. By doing this we can compare source performance independent of spectrometer bandwidth. The relationship is as follows, with numbered subscripts referring to different spectrometers;

$$c_{L,2}/c_{L,1} = \text{SBR}_1/\text{SBR}_2 = \Delta\lambda_{\text{eff},2}/\Delta\lambda_{\text{eff},1}$$

The relationship must be modified when  $\Delta\lambda_{\text{instr}} \leq 2\Delta\lambda_{\text{phys}}$ , as detailed by Boumans and Vrakking.<sup>30,31</sup> We can now compare the performance of the AGD used here to the performance expected of an ICP using the same spectrometer. We have

**Table 2** Comparison of AGD and ICP detection limits. Values not in parentheses are adjusted to match performance expected when using an identical spectrometer (0.1 nm bandpass), as was used in the present study. Values in parentheses are not adjusted for this. Wavelengths are as in Table 1 for the AGD and are those with the best reported  $c_L$  for the ICPs

Element	Adjusted $c_L$ in ppb (unadjusted $c_L$ in ppb)			
	AGD	Winge	Boumans	Activa
Cd	7	15 (3)	3 (0.5)	4 (0.3)
Mn	60	8 (1)	0.7 (0.1)	0.7 (0.06)
Mg	12	0.9 (0.2)	0.2 (0.03)	0.2 (0.02)
Cu	111	30 (5)	3 (0.5)	3 (0.4)

chosen to use three sets of ICP data for comparison. Detection limits from Winge *et al.*<sup>33</sup> have been included because they have often been used as standard values,<sup>1,34–40</sup> even though they are less impressive than the other sets of data. Detection limits from Boumans and Vrakking<sup>30</sup> are used because they have been recommended as standard values. For these data, the detection limits had to be standardized to the same  $k$  value (changed from  $2\sqrt{2}$  to 3). Detection limits from the Horiba Jobin–Yvon Activa promotional materials are used to reflect the performance of a modern commercial instrument and are very similar to those of Boumans and Vrakking. Physical line widths needed for the calculations are taken from Boumans and Vrakkers.<sup>41</sup>

Table 2 shows the experimentally determined detection limits for the AGD alongside the adjusted detection limits for these three ICPs. For Mn, Mg, and Cu, the detection limits with the AGD are one to two orders of magnitude worse than would be expected from an ICP with a similar spectrometer. For Cd, however, the AGD and ICP detection limits are comparable. The reason for the difference is that the other species are interfered with by molecular species in the AGD ( $\text{N}_2$  for Cu and OH for Mn and Mg), but only continuum is present in the region of Cd (see Fig. 5).

The disparity in detection limits points to the severity of the problem caused by background emission, and suggests that future studies should target this interference to improve performance. Better spectral resolution might lessen or remove these interferences, and should improve performance overall by reducing continuum emission. If background and analyte emission have different spatial patterns, spatial resolution would also improve performance. Some degree of isolation from the atmosphere should reduce  $\text{N}_2$  emission and possibly OH emission (although the latter partly, perhaps even largely, results from water in the sample). Further, changing the electrical, spatial, and flow parameters, which have not been extensively optimized at this point, might yield better results.

The demonstrated performance should be sufficient motivation for further study, including optimization, determination of other elements, coupling to separation techniques, and exploration of the effects of more complex samples (*i.e.*, matrix effects).

## Conclusions

A new, low power, low gas consumption, small footprint source for elemental analysis of solution samples has been

constructed. Although there is some increase in noise when an aerosol is introduced, the plasma remains stable under significant solvent loads. This solvent loading does appear to reduce the energy available for excitation; emission-based detection limits, using flow injection, ranged from 7 ppb (0.7 ng) for Cd to 111 ppb (11 ng) for Cu, among the metals measured. Linearity of a cadmium calibration is excellent over at least three orders of magnitude. The source shows significant promise as a low cost alternative to other higher power discharges.

## Acknowledgements

This research was supported by the US Department of Energy through Grant DE-FG02-98ER14890.

## References

- 1 *Inductively Coupled Plasmas in Analytical Atomic Spectrometry*, ed. A. Montaser and D. W. Golightly, VCH Publishers, Inc., New York, 2nd edn, 1992.
- 2 J. D. Ingle and S. R. Crouch, *Spectrochemical Analysis*, Prentice Hall, Upper Saddle River, NJ, 1988.
- 3 G. L. Moore, *Introduction to Inductively Coupled Plasma Atomic Emission Spectrometry*, Elsevier, New York, 1989.
- 4 J. A. C. Broekaert and V. Siemens, *Anal. Bioanal. Chem.*, 2004, **380**, 185–189.
- 5 J. Franzke, K. Kunze, M. Miclea and K. Niemax, *J. Anal. At. Spectrom.*, 2003, **18**, 802–807.
- 6 V. Karanassios, *Spectrochim. Acta, Part B*, 2004, **59**, 909–928.
- 7 W. C. Wetzel, F. J. Andrade, J. A. C. Broekaert and G. M. Hieftje, *J. Anal. At. Spectrom.*, 2006, **21**, 750–756.
- 8 T. Ichiki, T. Koidesawa and Y. Horiike, *Plasma Sources Sci. Technol.*, 2003, **12**, S16–S20.
- 9 J. Gubkin, *Ann. Phys. Chem.*, 1887, **32**, 114–115.
- 10 T. Cserfalvi, P. Mezei and P. Apai, *J. Phys. D: Appl. Phys.*, 1993, **26**, 2184–2188.
- 11 T. Cserfalvi and P. Mezei, *J. Anal. At. Spectrom.*, 2003, **18**, 596–602.
- 12 M. R. Webb, F. J. Andrade, G. Gamez, R. McCrindle and G. M. Hieftje, *J. Anal. At. Spectrom.*, 2005, **20**, 1218–1225.
- 13 R. K. Marcus and W. C. Davis, *Anal. Chem.*, 2001, **73**, 2903–2910.
- 14 W. C. Davis and R. K. Marcus, *Spectrochim. Acta, Part B*, 2002, **57B**, 1473–1486.
- 15 F. A. Andrade, W. C. Wetzel, G. C.-Y. Chan, M. R. Webb, G. Gamez, S. J. Ray and G. M. Hieftje, *J. Anal. At. Spectrom.*, 2006, **21**, 1175–1184.
- 16 V. I. Arkhipenko, S. M. Zgirovskii, A. K. Kapanik, L. V. Simonchik and D. A. Solov'yanchik, *Zh. Prikl. Spektrosk.*, 1998, **64**, 721–725.
- 17 Y. P. Raizer, *Gas Discharge Physics*, Springer, New York, 1997.
- 18 *Glow Discharge Spectroscopies*, ed. R. K. Marcus, Plenum Press, New York, 1993.
- 19 *Glow Discharge Plasmas in Analytical Spectroscopy*, ed. R. K. Marcus and J. A. C. Broekaert, John Wiley & Sons Ltd, West Sussex, 2003.
- 20 A. A. Yahya and J. E. Harry, *Int. J. Electron.*, 1999, **86**, 755–762.
- 21 J. L. Todolí, V. Hernandis, A. Canals and J.-M. Mermet, *J. Anal. At. Spectrom.*, 1999, **14**, 1289–1295.
- 22 J. Mora, S. Maestre, V. Hernandis and J. L. Todolí, *Trends Anal. Chem.*, 2003, **22**, 123–132.
- 23 K. B. Cull and J. W. Carnahan, *Spectrochim. Acta, Part B*, 1987, **42**, 629–635.
- 24 J. W. Novak and R. F. Browner, *Anal. Chem.*, 1980, **52**, 792–796.
- 25 J. Park, I. Henins, H. W. Herrmann and G. S. Selwyn, *J. Appl. Phys.*, 2001, **89**, 15–19.
- 26 E. Björn, T. Jonsson and D. Goitom, *J. Anal. At. Spectrom.*, 2002, **10**, 1257–1263.
- 27 T. D. Hettipathirana and D. E. Davey, *Appl. Spectrosc.*, 1996, **50**, 1015–1022.
- 28 R. M. Belchamber and G. Horlick, *Spectrochim. Acta, Part B*, 1982, **37**, 17–27.
- 29 J. W. Olesik, L. J. Smith and E. J. Williams, *Anal. Chem.*, 1989, **61**, 2002–2008.
- 30 P. Boumans and J. Vrakking, *Spectrochim. Acta, Part B*, 1987, **42**, 553–579.
- 31 P. Boumans and J. Vrakking, *J. Anal. At. Spectrom.*, 1987, **2**, 513–525.
- 32 J. M. Mermet, M. Carre, A. Fernandez and M. Murillo, *Spectrochim. Acta, Part B*, 1991, **46**, 941–952.
- 33 R. K. Winge, V. J. Peterson and V. A. Fassel, *Appl. Spectrosc.*, 1979, **33**, 206–219.
- 34 B. Knauth and M. Otto, *Fresenius' J. Anal. Chem.*, 2001, **371**, 1052–1056.
- 35 A. Lopez-Molinero, R. Gimenez, P. Otal, A. Callizo, P. Charmorro and J. R. Castillo, *J. Anal. At. Spectrom.*, 2002, **17**, 352–357.
- 36 K. Jankowski, *Microchem. J.*, 2001, **70**, 41–49.
- 37 A. Lopez-Molinero, A. Villareal, D. Andia, C. Velilla and J. R. Castillo, *J. Anal. At. Spectrom.*, 2001, **16**, 744–749.
- 38 A. C. Sahayam, *Fresenius' J. Anal. Chem.*, 1998, **362**, 285–288.
- 39 A. DeKlerk and R. J. Rademeyer, *J. Anal. At. Spectrom.*, 1997, **12**, 1221–1223.
- 40 A. L. Molinero, A. Morales, A. Villareal and J. R. Castillo, *Fresenius' J. Anal. Chem.*, 1997, **358**, 599–603.
- 41 P. Boumans and J. Vrakking, *Spectrochim. Acta, Part B*, 1986, **41**, 1235–1275.